Two-dimensional Fourier transform ESR correlation spectroscopy[a)]

Jeff Gorcester and Jack H. Freed
Baker Laboratory of Chemistry, Cornell University, Ithaca, New York 14853-1301

(Received 12 October 1987; accepted 8 January 1988)

We describe our pulsed two-dimensional Fourier transform ESR experiment and demonstrate its applicabilty for the double resonance of motionally narrowed nitroxides. Multiple pulse irradiation of the entire nitroxide spectrum enables the correlation of two precessional periods, allowing observation of cross correlations between hyperfine lines introduced by magnetization transfer in the case of a three-pulse experiment (2D ELDOR), or coherence transfer in the case of a two-pulse experiment (COSY). Cross correlations are revealed by the presence of cross peaks which connect the autocorrelation lines appearing along the diagonal $\omega_1 = \omega_2$. The amplitudes of these cross peaks are determined by the rates of magnetization transfer in the 2D ELDOR experiment. The density operator theory for the experiment is outlined and applied to the determination of Heisenberg exchange (HE) rates in 2,2,6,6-tetramethyl-4-piperidone-*N*-oxyl-d_{15} (PD-tempone) dissolved in toluene-d_8. The quantitative accuracy of this experiment is established by comparison with the HE rate measured from the dependence of the spin echo T_2 on nitroxide concentration.

I. INTRODUCTION

Fourier transform (FT) NMR has become commonplace because of its sensitivity advantage in comparison with continuous wave (cw) spectroscopy as well as for enabling two-dimensional spectroscopy, but the equivalent has not been true for ESR. Pulsed ESR spectrometers are usually limited to irradiation bandwidths which for most applications are too small for Fourier transform techniques. Broadband irradiation in ESR is now possible in certain cases because of new developments in microwave and digital electronics. The project of developing ESR instrumentation which will exploit the advantages of Fourier spectroscopy has been undertaken concurrently in several labs over the past several years.[1-4]

We have demonstrated the applications of two-dimensional electron spin echo (2D ESE) spectroscopy in studies of slow tumbling motions of nitroxide spin probes in both isotropic[5] and aligned[6] media as well as on surfaces.[7,8] This 2D ESE technique in its original form requires that one irradiate only a narrow band of the spectrum in any single repetition of the pulse sequence (i.e., highly selective pulses), alleviating the need for extremely narrow pulses and wideband detection systems. A related technique makes use of the three pulse stimulated echo sequence for observation of magnetization transfer processes driven by the stochastic tumbling motions of the spin probe.[9] Analysis of such 2D spectra are complicated somewhat by the need to model the effect of narrowband irradiation. They are also time consuming, requiring ~5–10 h for data acquisition.

By irradiating the entire spectrum using nonselective pulses (instead of slowly sweeping through it), 2D data acquisition times may be greatly reduced.[1] Even more interesting is that a nonselective pulse introduces coherence simultaneously to all spectral components, enabling the observation of coherence transfer between transitions. Transfer of coherence gives rise to cross correlations, which can only be distinguished from autocorrelations by having a true second frequency dimension. Such methods of correlation spectroscopy enable the observation of magnetization transfer between hyperfine (hf) lines, which manifests itself as cross correlations in a 2D correlation diagram of the coupled spin transitions. Related methods of correlation spectroscopy could also be applied to reveal coherence transfer between dipolar coupled nitroxides covalently attached to a single macromolecule. In summary, broadband irradiation of the entire spectrum offers substantial savings in data acquisition time, and at the same time has the potential of yielding much more information than analogous field-swept experiments.

We have introduced two-dimensional ESR correlation spectroscopy in a recent communication showing the application of these techniques to ESE and ELDOR spectroscopies.[1] Since that initial demonstration, our FTESR technique has undergone many important modifications and changes which have greatly improved its utility and accuracy. We present in this paper a detailed description of our FTESR method. We discuss the essential attributes of our spectrometer design which have helped us to realize our goal of performing two-dimensional ESR correlation spectroscopy. We then describe the pulse techniques which were previously unavailable to the ESR spectroscopist. Included, is a detailed experimental and theoretical description of our new 2D ELDOR technique for the *quantitative* determination of rates of magnetization transfer between hf lines, as illustrated in a study of Heisenberg spin exchange rates. We conclude with a brief discussion of the range of applicability of 2D FTESR.

II. EXPERIMENTAL ASPECTS

A. Microwave section of spectrometer

A block diagram of the spectrometer is given in Fig. 1. The microwave (MW) source consists of a reflex klystron which has been phase locked to a 15 MHz crystal oscillator. By maintaining a reflector voltage of 240 V, we obtain 320 mW output power with long-term frequency stability of at

[a)] Supported by NIH Grant No. GM-25862 and NSF Grant No. CHE 8703014.

 0021-9606/88/084678-16$02.10

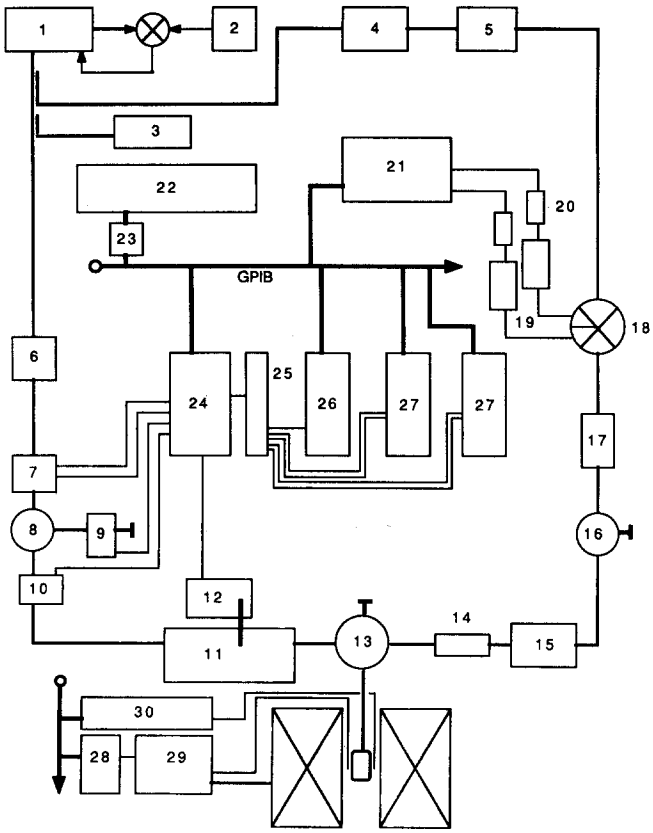

FIG. 1. Spectrometer block diagram. 1. Varian VA-297V klystron; 2.Microwave systems MOS frequency stabilizer; 3. Systron Donner 1255A frequency counter; 4. Systron Donner DBG-915 variable phase shifter; 5. Waveline 611 variable attenuator; 6. Waveline 612 variable attenuator; 7. Vectronix Microwave DP629.25HS digital phase shifter; 8. Western Microwave circulator; 9.,10. M/A-COM 96341 PIN diode SPST switches; 11. Litton 624 TWT amplifier; 12. modulator; 13. Junction Devices 115XHD circulator; 14. Hewlett Packard 33711A PIN diode limiter; 15. Narda Microwave N6244S-95 GaAsFET amplifier; 16. Western Microwave isolator; 17. Narda Microwave 4563 dc block; 18. Anaren 250270 quadrature IF mixer; 19. Comlinear CLC100 IF amplifiers; 20. Mini-Circuits BLP-300 low-pass filters; 21. Hewlett Packard HP54100A digitizing oscilloscope; 22. Digital Equipment LSI11/73 minicomputer; 23. National Instruments GPIBV11-2 DMA interface controller; 24. pulse control unit (PCU); 25. ECL OR gate and TTL→ECL converter; 26. Precision Instruments 9650 digital delay generator, modified for ECL output; 27. Berkeley Nucleonics 7030A digital delay generators; 28. Fieldial interface module (FIM); 29. Varian Fieldial Mark II field regulated magnet power supply; 30. Varian 929801 NMR gaussmeter.

least 1 part in 10^7. The MW radiation is passed through a calibrated variable attenuator and a 2-bit PIN diode phase shifter which has been optimized for operation at 9.25 GHz. The phase shifter PIN diodes are biased with TTL compatible drivers enabling MW transition times of 7 ns (10%–90% MW) and a 20 ns insertion delay (50% TTL–10% MW). MW pulse waveforms are generated with the aid of two PIN diode switches biased with emitter coupled logic (ECL) compatible drivers giving 1 ns rise times with 60 dB isolation. A circulator (item 8 in Fig. 1) incorporated into the switching network allows us to exploit the very short rise times of the PIN switches at both the leading and trailing edges of the MW pulse.

For generating MW power we employ a traveling wave tube (TWT) amplifier which has been modified to facilitate rapid direct anode modulation. Direct modulation of the TWT anode gives us gain switching rates of ~20 dB/ns, a rate sufficient to produce well defined 15 ns MW pulses without even using PIN diode switches, i.e., with continuous wave MW input to the amplifier. In the presence of MW pulses, the leading edge of the modulator pulse precedes the MW input pulse by ~10 ns and lasts until briefly after the MW pulse trailing edge. Rapid modulator switching eliminates the substantial noise power associated with the TWT amplifier after the MW pulse, which otherwise corrupts detection and increases spectrometer dead time. This system is capable of producing well defined pulses of 5 ns duration and dead times as short as 50 ns. Good results for many FT experiments and most narrowband irradiation ESE experiments can be obtained using the modulated TWT amplifier as the only means of MW pulse generation.[10] The modulator will be described elsewhere.[11]

The 1 kW MW pulses pass through a rotary-vane attenuator and are routed by a four port circulator to a TE102 mode rectangular cavity resonator. The cavity coupling hole (a centered circular iris) has been enlarged in order to reduce the loaded Q factor of the resonator (we henceforth refer to loaded Q as just "Q"). A brass screw inserted into the B field of the cavity allows tuneability of the resonant frequency. The half-power full bandwidth of the resonator can be estimated with the formula $\Delta\omega \sim \omega/Q$.[12] We estimate the Q of our resonator to be ~100, consistent with a half-power full bandwidth of 90 MHz (at 9.25 GHz) and a time constant of 3.4 ns; such a resonator will admit a pulse of duration as short as ~7 ns.[13] After loading the cavity, the resonant frequency is adjusted to 9.25 GHz for which the spectrometer operating conditions have been optimized.

MW signal is directed by the four port circulator into a PIN diode limiter. The limiter clips the waveform at 17 dB m in order to protect the GaAsFET amplifier from reflected power during a pulse. The low-noise amplifier (3.5 dB noise figure) provides 35 dB gain with saturated signal power exceeding 15 dB m. The amplified signal enters the MW port of a quadrature IF mixer (QIFM). The QIFM splits the MW with a 3 dB quadrature hybrid power divider, each output of which enters a mixer. The two mixers share the local oscillator (LO) signal derived from the homodyne reference arm. The IF outputs of the mixers should ideally be of equal amplitude and in phase quadrature; in practice, however, phase and amplitude imbalances in the hybrids and mixers result in deviations from phase quadrature and amplitude equality. The appearance of image peaks (reflections about the IF origin) in the ESR spectrum is a manifestation of phase and amplitude imbalances. An image peak may interfere with another resonance and cause a distortion of the ESR spectrum. The magnitude of an image peak relative to its parent peak defines the image rejection of the QIFM.[14] Typical commercial QIFM's specify an image rejection of −20 dB, a value we have found to be insufficient for ESR applications. To circumvent the shortcomings of the quadrature detector we apply an image cancellation phase alternation sequence known as CYCLOPS.[15] We record four FID's with relative MW phases of 0°, 90°, 180°, and 270°. An appropriate linear combination of the four complex time series amounts to an orthonormalization of the FID,

provided that the MW phase shifts are very precise, and that the insertion loss of each PIN diode phase shifter is not too severe. To guarantee the precision of our phase shifts, we operate the spectrometer within a frequency band (9.25 ± 0.05 GHz) for which our digital phase shifter has been optimized. Within this range we obtain image rejection of 40 dB.

B. Digital electronics

A general purpose interface bus (GPIB, IEEE std. 488-1978) interconnects an 18 MHz LSI11/73 minicomputer with the spectrometer instrumentation. Communication between the LSI bus and the GPIB is facilitated by a direct memory access (DMA) interface controller supporting data transfer rates of 500 kbytes/s. Because of the large amount of data collected in a 2D experiment, the data transfer time constitutes a significant fraction of the total data collection time. Transient recorders are usually limited to data transfer rates of well below 500 kbytes/s and should be selected with attention to this specification. 2D data acquired on the LSI11 is transferred to a 32-bit Sun Microsystems 3/60 workstation via thinwire ethernet. A 2D data file containing 200 complex FIDs can be transferred in 7 s. Fourier transformation and graphical presentation of 2D data is performed by the Sun work station, thereby freeing the LSI11 for further data acquisition.

Timing of the logic control pulses to the PIN diode switches, modulator, and digital phase shifters is facilitated by a pulse control unit (PCU). The PCU is interfaced to the minicomputer via the GPIB with the aid of a Fairchild 96LS488 integrated GPIB controller. The interface allows rapid programmability of the number of MW pulses (as many as 15) and a four-bit pattern associated with each pulse, which determines the TTL logic states of four external devices during that pulse. Data are stored in successive locations of a 16×4, 15 ns RAM. A four-bit word is retrieved from location $\mathbf{n}$ synchronously with the trailing edge of MW pulse number $\mathbf{n}-\mathbf{1}$. In this way the PCU can modify the external logic signals well before the MW pulse. The RAM address pointer is reset following the final pulse of a sequence by a one-shot timeout circuit. Two of the external logic signals are reserved for the digital phase shifter, while the other two are for options such as a digital attenuator. The timebase of the PCU is established by a train of ECL pulses from the digital delay generators.

Computer control of the dc magnetic field is facilitated by a Fieldial interface module (FIM). The FIM receives two bits of data from the 11/73. Each bit controls a relay connected in parallel with the sweep-up or sweep-down front-panel switches on the Fieldial Mk. II. By monitoring the absolute field with a GPIB-interfaced NMR gaussmeter, we obtain a field setability of 1 part in 10^6, or roughly 30 mg at X band. Photodiodes provide optical isolation between the relays and the FIM to protect the FIM against spikes generated by relay contact closures.

C. Data acquisition

The fundamental theorem in the discrete representation of continuous functions is the familiar Nyquist sampling theorem.[16] Consider the case of the undamped sinusoid, i.e., a signal represented by a single Fourier component. The discrete representation of a sinusoid of frequency f_s Hz requires that we sample the function at least every $1/2f_s$ s, giving a sampling rate $f_{\rm smp}$ of $2f_s$. It is standard practice to define the Nyquist frequency $f_{\rm Nq}$ to be the highest frequency Fourier component that can be accurately reconstructed with a given sampling rate. Thus $f_{\rm Nq} = \frac{1}{2} f_{\rm smp}$. A sinusoid of frequency $f_{\rm Nq} + \Delta f$ will be represented in Fourier space by a peak at $f_{\rm Nq} - \Delta f$ when reconstructed from the discrete set of samples; this phenomenon, known as aliasing, can be avoided by proper application of the sampling theorem. Damping of the sinusoid introduces Fourier components at frequencies higher than f_s, thereby increasing the necessary sampling rate.

The sampling theorem establishes a lower bound to $f_{\rm smp}$, but does not address determination of an optimum sampling rate. Optimal sensitivity will be attained with strict application of the sampling theorem only in the hypothetical case of a noiseless signal sampled with infinite analog-to-digital converter (ADC) resolution. Mehlkopf *et al.*[17] have shown that the power density of the digitization noise goes as $\sim q^2/f_{\rm smp}$, where q is the digitization step. Thus, sampling in excess of the required rate reduces the rms noise power associated with digitization (analogous to the use of several channels to record the same signal). Now consider noise at the input to the ADC accompanying FID signal components of frequency no greater than f_s. Stationary white noise consists of Fourier components which extend in frequency well beyond f_s. Noise components at frequencies beyond $f_{\rm Nq}$ will be aliased, thereby increasing the noise power in the vicinity of the signal components. This will be the case, in practice, when the Nyquist frequency, established by the sampling rate, is lower than the IF frequency cutoff of the spectrometer detection system. Thus, for instance, if the IF bandwidth of the spectrometer is limited by the analog bandwidth $f_{\rm tr}$ of the transient recorders, then a Nyquist frequency $f_{\rm Nq} = f_{\rm tr}$ would give the optimum noise rejection. In the case of unlimited ADC and computer wordlengths, no gain in sensitivity would be achieved with further increase in $f_{\rm Nq}$.[18]

An alternative to adjustment of the sampling rate is limitation of the detector bandwidth. This is easily accomplished by placement of a low-pass filter at each IF output of the quadrature mixer. Optimal noise rejection requires the implementation of one (or both) of the following: (1) transient recorders with variable sampling rates, or (2) low-pass filters with variable frequency cutoff. The two methods of noise rejection achieve the same sensitivity (assuming negligible digitization noise); the method of choice for a particular application is entirely a matter of experimental convenience provided the bandwidth achieved is consistent with the spectral width of the signal. The conversion rate of integrated analog-to-digital converters is usually fixed by the manufacturer, thus commercial transient recorders seldom have adjustable sampling rates. Some digitizing oscilloscopes can interleave successive sweeps, thereby increasing the effective sampling rate. In the case of the HP scope used in our experiments, the technique of interleaving has been implemented in a manner that allows continuous variability of the effec-

tive dwell time over the range 10 ps to ~1 s.[19] Interleaving of repetitive waveforms is performed at the cost of reducing the "effective" sweep rate of the digitizers (i.e., the number of averages of the fully interleaved data per unit time). Unlike the case for NMR, where the experimental repetition rate is usually established by the nuclear T_1, the repetition rate for an ESR experiment is most often determined by the (real time) sweep rate of the transient recorders. Thus, even if the sampling rate can be continuously varied, it is nevertheless advantageous to bandwidth limit the detector in order to maintain a high effective sweep rate.

The HP scope we have used is perhaps not the ideal instrument for FTESR data acquisition, but it is a useful compromise. The 25 ns dwell time of the HP digitizers is insufficient to reconstruct an FID with signal components exceeding 20 MHz. That is, a real time sampling rate of 40 Msamples/s (25 ns dwell time) limits the accessible single shot spectral bandwidth to 40 MHz (with quadrature detection). It is most often the case for ESR of nitroxides that spectral bandwidths exceed this limit. To achieve higher effective sampling rates the HP scope, as already noted, interleaves many successive sweeps in order to represent a "single-shot" waveform. The FIDs described in this report typically consist of Fourier components as high in frequency as $\pm$ 60 MHz, so that we typically use an effective dwell time of between 5 and 10 ns.

A transient recorder which performs conversions at rates of 200 Msamples/s or greater will adequately record such FID's in a single sweep. Such digitizers are available in the form of CAMAC modules but are limited to sweep rates not exceeding about 200 sweeps/s in signal averaging applications.[20] The HP scope is capable of slightly higher sweep rates (about 300 sweeps/s) but must interleave successive sweeps to achieve the required effective dwell time. The CAMAC transient recorders provide very good performance for dedicated data acquisition if one requires no more than $\pm$ 100 MHz bandwidth (for spectra ~200 MHz in width). The HP scope has a much higher analog bandwidth (1 GHz) than the transient recorders we refer to above, so that with its variable effective dwell time, it is a more flexible instrument suitable for a wider range of applications. Ideally one should have several instruments, e.g., CAMAC transient recorders for data conversion, and a 1 GHz sampling oscilloscope (such as the HP54100A) for test and measurement (e.g., of the MW pulse shapes) and for recording spectra exceeding 200 MHz bandwidth. The HP54100A represents a compromise in that data conversion and high speed measurement can be accomplished economically with a single instrument, and higher effective sampling rates can be accommodated as they become necessary.

Free precession of the electronic magnetization follows irradiation of the sample with a short 9.25 GHz MW pulse. The signal appears at the GaAsFET amplifier as an amplitude modulated 9.25 GHz waveform. Downconversion of the free precession signal yields time varying voltages at the IF ports of the quadrature detector which are digitized by the sampling oscilloscope. Signal averaging is performed within the HP scope and the average FID is dumped directly to LSI11 memory via the GPIB and DMA interface. A 256 point/channel FID recorded with a dwell time of 5.0 n and averaged 128 times (i.e., averaging of fully interleaved FID's) can be recorded in 3.8 s from command line entry into the computer to storage of the data on the disk. This is more than sufficient signal averaging for collection of a spectrum such as that shown in Fig. 2. The spectrum obtained from FT of the FID is equivalent to the (frequency swept) ESR spectrum obtained by slow-passage techniques. FT of an averaged FID (consisting of in-phase and quadrature signals) will produce a spectrum corrupted by mirror images arising from imperfect quadrature detection. In order to obtain imageless spectra we use the CYCLOPS image cancellation sequence. FT of the FID recorded with CYCLOPS will give the correct frequency spectrum, but an admixture of absorption and dispersion.[15] To project out the pure absorption representation of the ESR spectrum, frequency-dependent phase corrections must be applied. These corrections are necessary due to the dead-time delay before sampling of the FID following the initiation of free-precession.[4] There will be some attenuation and additional phase shifts if the spectral bandwidth exceeds $2\gamma_e B_1$, where B_1 is the MW field strength (see below).

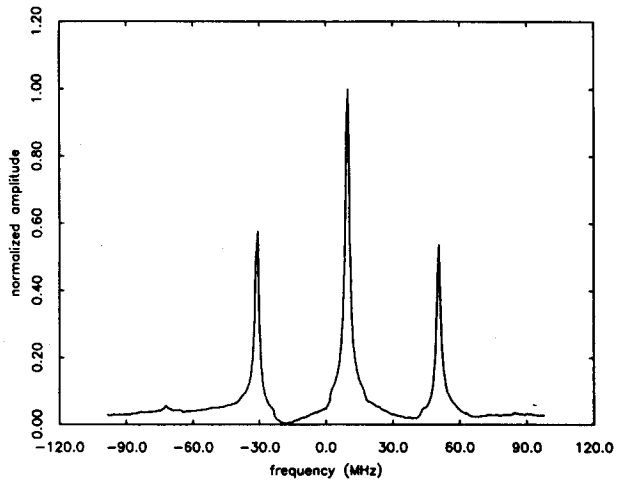

FIG. 2. Absolute value FT spectrum of 5.1×10^{-4} M PD-tempone in toluene-d_8 at 21°; obtained from the average of 40 FIDs, each consisting of 256 complex data points extending to 1.2 μs; t_p = 14 ns corresponding to $B_1 \sim 6$ G. The data has not been amplitude corrected (see the text).

Two-dimensional spectroscopy requires that one apply several MW pulses and record the FID or ESE following the final pulse, during the so called detection period (cf. Fig. 5). The sampling theorem must again be employed in selecting an appropriate incremental t_1 (which is the time between the first and second MW pulses). It is desirable to have the same sampling rate in both t_1 and t_2 (cf. Fig. 5) so that the frequency resolution is the same (assuming the same zero-filled extension) in both dimensions of the 2D spectrum. Because of constraints on computer storage and data collection time it is often preferable to use the maximum incremental t_1 consistent with the sampling theorem. CYCLOPS and other phase alternation sequences are performed at each t_1 time step, with the appropriate linear combinations of FIDs computed at run time in order to minimize storage requirements. A typical 2D experiment involves sophisticated phase alter-

nation schemes (see below), requiring the collection of about 3000 averaged FID's, each consisting of 256 complex data words. This sequence of operations is controlled by the LSI11 minicomputer and requires 15–30 min per 2D spectrum. The main program segment is written in Fortran-77 for ease of modification. Time critical tasks and tasks which require access to the I/O page have been written in macro assembly language to minimize system overhead.

In many applications of ESE spectroscopy it is sufficient that the MW pulses excite only a narrow portion of the ESR spectrum. The amplitude of the spin echo is recorded as a function of the interpulse delay, and if desired, the experiment is repeated after incrementing the dc magnetic field. An acceptable technique for recording partial excitation spin echoes is to gate the echo with a sample-and-hold aperture, accumulating charge on a capacitance over many repetitions of the pulse sequence. This is the concept of the familiar "boxcar" integrator. For data acquisition using the gated integrator we have constructed an LSI bus divide-by-N clock which synchronizes the spectrometer (i.e., the PCU) with the 11/73. The CPU enters the requested count into the clock interface via the LSI bus. Clock pulses from the external timebase pass through the divide-by-N clock en route to the boxcar sample-and-hold aperture trigger. When the count reaches the preprogrammed value, trigger pulses to the boxcar are suspended, the divide-by-N clock interrupts the 11/73, and a conversion of the analog boxcar output is performed by a 12-bit LSI bus A-to-D converter. Time delays and phases are updated via the GPIB before the next countdown sequence is initiated. For acquisition of a two-pulse envelope, we alternate the phases of the MW pulses between 0,0 and 180,0 following each A-to-D conversion in order to achieve optimal cancellation of unwanted coherences (such as FID) which do not refocus with the spin echo.

D. Fourier spectroscopy

In the ideal single pulse experiment, a MW pulse of duration t_p rotates the equilibrium magnetization through an angle

$$\beta = \gamma_e B_1 t_p = \pi/2 \tag{1}$$

about the direction of the applied field $\mathbf{B}_1$ irrespective of the resonance offset. This is approximately the case when the resonance offset does not exceed the strength of the MW field, i.e., when

$$|\omega_0 - \omega_{rf}| < |\gamma_e B_1| \tag{2}$$

and when $t_p \ll T_2$. The spectral bandwidth of nitroxides at X band is determined by the hf coupling and may be as large as 220 MHz (e.g., for very slow motional spectra). The isotropic hf coupling in nitroxides is about 15 G, implying a total (motionally narrowed, isotropic) spectral bandwidth of about 90 MHz. Because of the large resonance offsets encountered in nitroxides, we are rarely able to obtain sufficient MW field strength at the sample to satisfy Eq. (2); thus the need to consider off-resonance effects. The magnetization is rotated about an effective $\mathbf{B}_1$ that is tilted with respect to the z axis by an angle

$$\theta = \tan^{-1}\left(\frac{B_1}{B_0 - \omega_{rf}/\gamma_e}\right) \tag{3}$$

and has the amplitude

$$B_{eff} = [B_1^2 + (B_0 - \omega_{rf}/\gamma_e)^2]^{1/2}. \tag{4}$$

With a low Q cavity resonator, we find that we are limited in practice to a pulsewidth of no less than 14 ns because of insufficient transmitter power to satisfy Eq. (1) in the case of shorter t_p. Although we can generate 5 ns MW pulses with 1.2 kW peak power, only small pulse rotations ($\beta < \pi/2$) may be achieved because of the inefficient conversion of incident power into B_1 at the sample in a cavity. The conversion efficiency may be improved by confinement of the B_1 field,[21] e.g., with a loop-gap resonator[22] stabilized against electric breakdown.[23] A 14 ns pulse with $\beta = \pi/2$ on resonance corresponds to a B_1 of about 6 G, or uniform spectral rotation over a bandwidth of about 34 MHz ($2\gamma_e B_1$). It would seem that a 6 G B_1 would be insufficient for wideband excitation of nitroxides. Good results for motionally narrowed spectra can be obtained, however, because of the slow falloff of the amplitude response $(M_x^2 + M_y^2)^{1/2}$ as the resonance offset is increased beyond $\gamma_e B_1$.[4,24] The amplitude response predicted by Eqs. (3) and (4) falls off to 50% at an offset of about $2.7\gamma_e B_1$, implying a "half-amplitude response" bandwidth of $5.4\gamma_e B_1$, or about 90 MHz for a B_1 of 6 G. Amplitude and phase distortions which occur when the total spectral bandwidth exceeds $2\gamma_e B_1$ can be corrected numerically. Figure 2 illustrates a spectrum obtained from the FID; the same spectrum recorded by the slow-passage technique has three hf lines of nearly equal amplitude; each of the outer hf lines of the FT spectrum are reduced $\sim 50\%$ in amplitude. Although this result is in apparent agreement with the predicted falloff of the response of the magnetization, we note that the signal voltage at the detector associated with each of the outer hf lines is reduced because of the limited bandwidth of the resonator (see below), so that the actual half-amplitude response bandwidth is somewhat greater than that predicted by the classical description given above for an ideal rectangular pulse. We have numerically solved the Bloch equations utilizing the experimental pulse shapes, and we obtain better agreement with the observed FT spectrum. The classical description of Eqs. (3) and (4) is nevertheless useful in estimating the off-resonance amplitude response. The equilibrium magnetization is rotated through an angle $\beta_{eff} = \gamma_e B_{eff} t_p$ about $\mathbf{B}_{eff}$; resulting in a projection on the xy plane with amplitude and phase depending on resonance offset.[4,25] A null in the amplitude response occurs when the effective rotation angle β_{eff} is some integer multiple of 2π, such that the magnetization is rotated about $\mathbf{B}_{eff}$ until restored to its original state.

The phase of the magnetization immediately after a MW pulse varies with resonance offset in a manner described by

$$\phi = \tan^{-1}\left[\frac{(\omega_0 - \omega_{rf})(1 - \cos\beta_{eff})\sin\theta}{\gamma_e B_1 \sin\beta_{eff}}\right], \tag{5}$$

where θ is the tilt angle given by Eq. (3). Numerical evaluation of Eq. (5) indicates that the phase angle increases al-

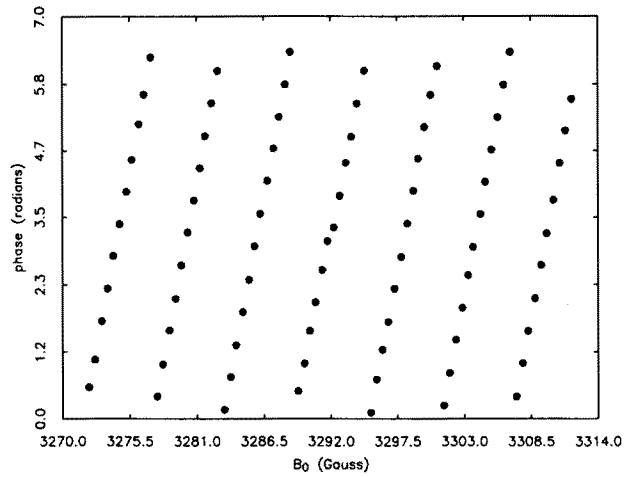

FIG. 3. Phase shift of the $M_I = 0$ line of the spectrum of Fig. 2 determined as a function of resonance offset $B_0 - \omega_{rf}/\gamma_e$; where the carrier frequency ω_{rf} was fixed corresponding to a resonance field of 3292.1 G.

most linearly with resonance offset. The observed phase response of the apparatus is shown in Fig. 4. The phase is found to vary linearly over a 120 MHz bandwidth centered at ω_0 with a proportionality factor α of 0.398 rad s. An additional contribution to the frequency dependent phase error shown in Fig. 3 accumulates during the spectrometer dead time τ_d and is described by $\phi(\omega_0 - \omega_{rf}) = (\omega_0 - \omega_{rf})\tau_d/2\pi$.

E. Sensitivity

The sensitivity advantage of Fourier spectroscopy in comparison with slow-passage experiments in NMR is well documented.[26,27] We illustrate the sensitivity of our spectrometer with the FID of Fig. 4. Using a six-bit, 1 gsample/s digitizer[28] we recorded a single-shot FID of 5×10^{-4} M PD-tempone in toluene-d_8 with 2048 samples and a 1 ns dwell time; the signal/noise ratio of this FID (i.e., the ratio of the maximum FID signal voltage to the rms noise voltage determined from the base line) is found to be 86. The signal/noise ratio of the spectrum obtained upon FT of this FID was estimated to be 100, taking the height of the properly phased absorption line nearest resonance as the signal amplitude, and the rms value of the base line as the noise amplitude. We estimate that the FT spectrum after 30 s of signal averaging (with our HP54100 scope) has a S/N$\sim$4200; this is to be compared with a S/N$\sim$400 that we have obtained from the same sample solution by conventional cw methods with a 30 s scan time. (Digitizers with higher sweep rates than the HP54100 would, of course, give correspondingly greater S/N for the same acquisition time.)

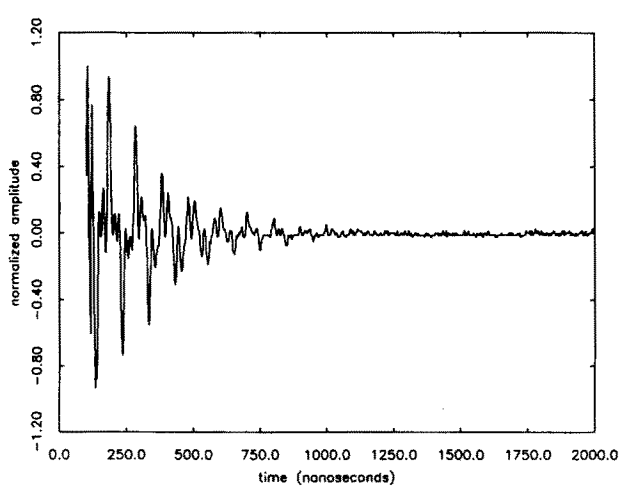

FIG. 4. Single shot FID of 5.1×10^{-4} M PD-tempone in toluene-d_8 at 21°; obtained with 1 ns time resolution with a dead time of $\sim$90 ns; $t_p = 12$ ns. The signal/noise ratio of this FID is found to be 86 (see the text).

In comparing the sensitivity of Fourier spectroscopy with that of conventional slow passage techniques, the former is considered analogous to having a multichannel cw spectrometer. Each Fourier component of the MW pulse produces an impulse response determined by the value of the spectrum at its frequency.[24] The sensitivity advantage of Fourier spectroscopy is in a qualitative sense governed by the number of channels which simultaneously record a spectral component. We do not attempt to formulate a quantitative sensitivity comparison of the two techniques. The principal objective of this report is to investigate methods of 2D ESR correlation spectroscopy which require that coherence be simultaneously introduced to all spectral components. An important part of this investigation is the optimization of experimental conditions. We present a brief discussion of sensitivity as it pertains to experimental optimization, drawing extensively from similar treatments in NMR[24,26,27,29] while accounting for some fundamental differences between NMR and ESR.

We assume a resonant signal of the form

$$s(t) = a\exp(-t/T_2^*)\exp(-i\omega t), \tag{6}$$

where ω is the precessional frequency in the rotating frame, T_2^* is the decay time of the FID, and a is the amplitude given by $\epsilon M_0 \exp(-\tau_d/T_2^*)$, where τ_d is the dead time of the spectrometer, and ϵ is a spectrometer constant (we neglect off-resonance effects for the sake of simplicity). The signal voltage at the detector is then

$$V_s(t) = a\exp(-t/T_2^*). \tag{7}$$

It is customary in NMR to multiply the signal by the weighting function $\exp(t/T_2^*)$, corresponding to matched convolution filtering in the frequency domain. We do not perform this step in ESR because of the importance of preserving the spectral line shape.[30] We assume the coherent addition of n complex free induction decays (i.e., signal averaging), each represented by M equidistant samplings between 0 and τ. The peak amplitude in the corresponding spectrum is obtained by the Fourier transform

$$S = \mathcal{F}\{V_s(t)\}_{\omega=0} = \frac{nMa}{\tau}\int_0^\tau \exp(-t/T_2^*)dt, \tag{8}$$

where we have approximated the sum over the M samplings in the discrete Fourier transform by an integral. We assume the noise is white and is limited by the low pass filters of cutoff f_c; the rms noise voltage V_n is then a constant proportional to the square root of f_c, i.e., $V_n = pf_c^{1/2}$, leading to the

ratio

$$\frac{V_s}{V_n}=\frac{naMT_2^*}{pf_c^{1/2}\tau}\left[1-\exp(-\tau/T_2^*)\right]. \tag{9}$$

To avoid additional noise amplitude due to aliasing of high frequency noise components, we set f_c equal to the Nyquist frequency $f_{\rm Nq}=M/2\tau$ leading to

$$\frac{V_s}{V_n}=\frac{naT_2^*}{p}\left(\frac{2M}{\tau}\right)^{1/2}\left[1-\exp(-\tau/T_2^*)\right]. \tag{10}$$

We are primarily concerned with the final signal/noise ratio after signal averaging for some fixed time $T=nT_{\rm rep}$, where $T_{\rm rep}$ is the time between successive repetitions of the pulse sequence. We define an effective power signal/noise ratio[29] as

$$\frac{S}{N}=\left(\frac{V_{s,T}}{V_{n,T}}\right)^2 T \tag{11}$$

and relate the sensitivity to the square root of the power signal/noise ratio per unit time[24]

$$\left(\frac{S}{NT}\right)^{1/2}=\frac{V_{s,T}}{V_{n,T}T^{1/2}}=\frac{aT_2^*}{p}\left(\frac{2Mn}{\tau T_{\rm rep}}\right)^{1/2}\left[1-\exp(-\tau/T_2^*)\right]. \tag{12}$$

In order to obtain good line shapes and avoid the use of apodizing filters, we require that the signal decay to 1% of its initial value; this is consistent with $\tau/T_2^*=\ln(100)\sim 5$ and gives the simple result

$$\left(\frac{S}{NT}\right)^{1/2}=\frac{M_0\epsilon}{5p}\left(\frac{2Mn\tau}{T_{\rm rep}}\right)^{1/2}\exp(-\tau_d/T_2^*). \tag{13}$$

The factor $\tau/T_{\rm rep}$ represents the duty cycle of the receiver, M represents the effective number of samplings, and n represents the reciprocal of the number of sweeps interleaved by the digitizers in order to achieve the effective sampling rate M/τ.

We have thus far assumed $T_{\rm rep}\gg T_1$ because of duty cycle limitations of the transient recorders. This will not always be the case, however, since T_1's on the order of seconds have been observed in selected systems. If $T_1\geqslant 1/d$, where d is the maximum sweep rate of the transient recorders, $T_{\rm rep}$ must be increased to avoid saturation of the spin system. In these cases an optimization of the sensitivity with respect to $T_{\rm rep}$ yields the optimal $T_{\rm rep}$ given by the approximate ratio $T_1/T_{\rm rep}\simeq 0.79$.[21] For a single pulse FID experiment it may also be desirable, in the case of $T_1>1/d$, to reduce the pulse rotation angle β below $\pi/2$ in order to more rapidly achieve equilibrium populations following detection. We refer the reader to the NMR literature for a more detailed discussion of these topics.[24,26,29]

We have not yet considered the effect of resonator Q on sensitivity. We proceed with the analysis taking ϵ in Eq. (13) to represent the spectrometer with $Q=1$. Consider the case of a spectrum consisting of a single resonance line of Lorentzian shape and of width $2/T_2^*$. We expect an enhancement of sensitivity with higher Q since less of the signal energy is dissipated through the resonator walls, thus providing greater signal voltage at the detector. Mims has shown that the sensitivity in ESE spectroscopy is approximately proportional to $Q^{1/2}$.[21] Since the echo height and the height of an FID are nearly equivalent, his analysis and result would also apply to the FID's. We therefore multiply the right side of Eq. (13) by $Q^{1/2}$ to obtain

$$\left(\frac{S}{NT}\right)^{1/2}=\frac{M_0\epsilon}{5p}\left(\frac{2Mn\tau}{T_{\rm rep}}\right)^{1/2}Q^{1/2}\exp(-\tau_d/T_2^*). \tag{14}$$

We assume that resonator ringing is the only source of spectrometer dead time (although other factors such as recovery of limiter and low noise amplifier affect the observed dead time) and that a decay m (dB) typically of the order of 140 dB is needed to reduce the power level to that of noise.[21,31] The power in the resonator decays as $\exp(-\omega_{\rm rf}t/Q)$, where the resonator is tuned to $\omega_{\rm rf}$, thus we obtain

$$\tau_d\simeq\frac{m}{10}(\log_e 10)\frac{Q}{\omega_{\rm rf}}\simeq 32\frac{Q}{\omega_{\rm rf}}. \tag{15}$$

Substituting for τ_d in Eq. (14), and optimizing with respect to Q gives the expression

$$Q_{\rm opt}=\omega_{\rm rf}T_2^*/64 \tag{16}$$

with the resonator tuned to the transmitter frequency ω. It follows from Eq. (15) that at $Q_{\rm opt}$, $\tau_d\simeq T_2^*/2$ (independent of m). Hence for a resonance line of $T_2^*=100$ ns, with $\nu=10$ GHz, we expect optimal sensitivity in the FID experiment with $Q=100$ (Ref. 32) and $\tau_d\simeq 50$ ns. If the spectrum consists of more than one resonance line we impose the additional constraint that the resonator half-power bandwidth be at least as large as the spectral bandwidth.[33] Hence for the case of a motionally narrowed nitroxide spectrum of width 100 MHz, with $T_2^*=200$ ns (for each hf line) and $\nu=10$ GHz, we must reduce the Q from $Q_{\rm opt}=200$ to a Q of 100 in order to insure adequate sensitivity to off-resonance spectral components.

Implementation of these concepts for nitroxide studies requires that Q, B_1, and hence transmitter power be continuously variable over a range which is not always experimentally feasible. In order to maintain a constant B_1 at the sample, halving the Q requires an associated doubling of the power to the resonator; a step which is ultimately limited by saturation of the MW transmitter amplifier. The transmitter power and resonator Q needed to achieve coverage of a spectrum of given bandwidth can be deduced from steady-state arguments with the expression

$$P_0=\mu_0 V_c B_1^2\nu/2Q \tag{17}$$

relating B_1 at the sample to MW power P_0 dissipated by the resonator, and loaded resonator Q; ν is the resonator frequency and V_c is the effective cavity volume.[21,34] P_0 is equal to the MW power incident on the resonator if the resonator is matched.[35] The half-power full bandwidth of the resonator is given approximately by ν/Q, while the half-amplitude response bandwidth is estimated by $\Delta\nu\sim 5.4\gamma_e B_1/2\pi$. Thus we see from Eq. (17) that the required transmitter power is cubic in the desired bandwidth. Fixing the available transmitter power, we achieve optimal spectrometer performance by adjusting t_p and Q until the half-power resonator band-

width is equal to the half-amplitude response bandwidth. In the present apparatus this corresponds to a B_1 of 6 G (t_p = 14 ns) and a Q of 100 when operating with the maximum available transmitter power of 1.2 kW. In order to double the spectrometer bandwidth we need an increase in transmitter power by a factor of 8. Alternatively we can decrease the effective cavity volume by the same factor, which is easily accomplished with a loop-gap resonator.

F. Two-dimensional correlation spectroscopy

Two-dimensional correlation spectroscopy (COSY) in its various forms has gained widespread use in NMR as a method of observing coherence transfer between coupled spin transitions. The pulse sequence $\pi/2$–t_1–$\pi/2$–t_2 constitutes the simplest of the COSY experiments and is used in NMR in the separation of scalar interactions.[36] A COSY ESR spectrum is obtained in much the same manner as for NMR; the basic pulse scheme is illustrated in Fig. 5. The preparation period consists of a $\pi/2$ pulse to generate the initial transverse magnetization components. Free precession of the magnetization occurs during the evolution period of duration t_1 during which the components become "labeled" according to their precessional frequencies in the rotating frame. The FID is recorded during the detection period of duration t_2, which begins with the final $\pi/2$ pulse. For each t_1 the FID is collected, then the phase of the first pulse is advanced by 90°, and a second FID is collected. These two signals depend on terms oscillatory in t_1 that are in phase quadrature (cf. Sec. III).[37] Two-dimensional complex Fourier transformation generates a spectrum over two frequency variables, ω_1 and ω_2.

This two step 2D quadrature phase alternation sequence yields the required frequency discrimination in ω_1, and it provides the phase information necessary for the pure absorption representation of the 2D spectrum.[38] A full 2D image cancellation sequence requires that we combine this two step procedure with the four step CYCLOPS image cancellation method to obtain a sequence consisting of eight steps. Table I illustrates this eight step sequence by giving the phase of each MW pulse and the deposition of channel 1 and channel 2 data into four possible memory locations. A

TABLE I. Phase alternation sequence for 2D COSY ESR.

Step	Phase[a]		Memory address[b]			
	ϕ_1	ϕ_2	1	2	3	4
1	x	x	+1	+2		
2	y	y	−2	+1		
3	$-x$	$-x$	−1	−2		
4	$-y$	$-y$	+2	−1		
5	y	x			+1	+2
6	$-x$	y			−2	+1
7	$-y$	$-x$			−1	−2
8	x	$-y$			+2	−1

[a] The phase of each MW pulse in the two pulse sequence.
[b] There are four distinct arrays into which data from the two digitizer channels are either added (+) or subtracted (−).

COSY ESR spectrum of 5×10^{-4} M PD-tempone in toluene-d_8 obtained in this manner is shown in Fig. 6. Resonances at positions for which $\omega_1 = \omega_2$ will be referred to in the standard fashion as autopeaks because they represent autocorrelations. Cross peaks representing cross correlations are not found in the spectrum of Fig. 6 because of the weakness of the electron–electron dipolar and chemical or Heisenberg exchange interactions.[39] Additional peaks at positions for which $\omega_1 = 0$ arise because of electron spin flips during the evolution period; these peaks are referred to in the standard manner as axial peaks.[36]

2D exchange correlation spectroscopy is a variant of the COSY method which incorporates a third $\pi/2$ MW pulse to examine the transfer of magnetization between hf lines, as we have shown for the mechanism of Heisenberg spin exchange.[1] We refer to this experiment as 2D ELDOR spectroscopy because of its close relationship to that double resonance method. 2D ELDOR involves a procedure similar to

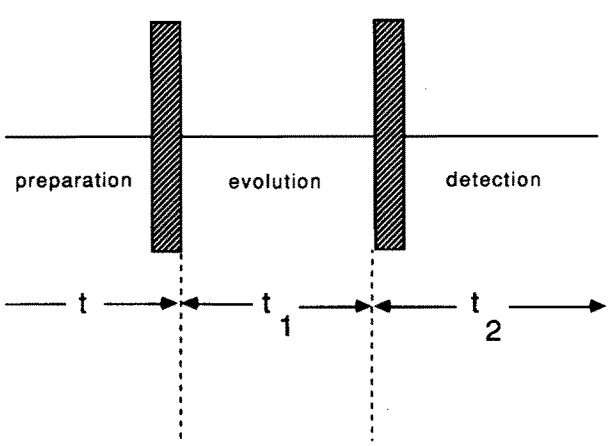

FIG. 5. 2D COSY pulse sequence.

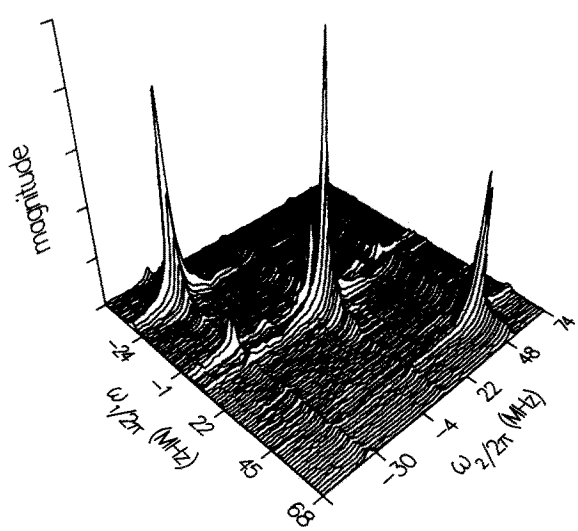

FIG. 6. Absolute value 2D COSY ESR spectrum of 5.1×10^{-4} M PD-tempone in toluene-d_8 at 21°; t_p = 15.5 ns; Δt_1 = 6 ns; Δt_2 = 3.9 ns; $90t_1$ steps; eight step phase alternation sequence with 30 averaged FID per step; dead time in t_2 of 100 ns; dead time in t_1 of 120 ns; acquisition time 10.6 min.

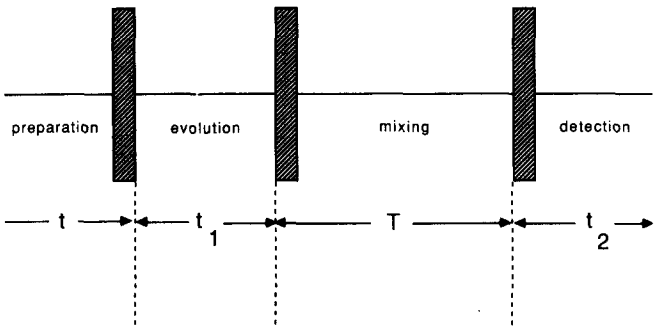

FIG. 7. 2D ELDOR pulse sequence The pulse sequence for 2D ELDOR involves four time periods: preparation, evolution, mixing, and detection. The preparation period consists of a $\pi/2$ pulse to generate the initial transverse magnetization. "Frequency labeling" occurs during the evolution period of duration t_1. The second $\pi/2$ pulse starts the mixing period wherein the longitudinal magnetization components associated with each hf line can be exchanged, thereby mixing components carrying different precessional frequency information. Thus, after rotating this magnetization into the xy plane for detection, components initially precessing with angular frequency $\omega_1 = \omega_a$ will, to the extent that magnetization transfer has occurred during the mixing period, precess with new angular frequency $\omega_2 = \omega_b$.

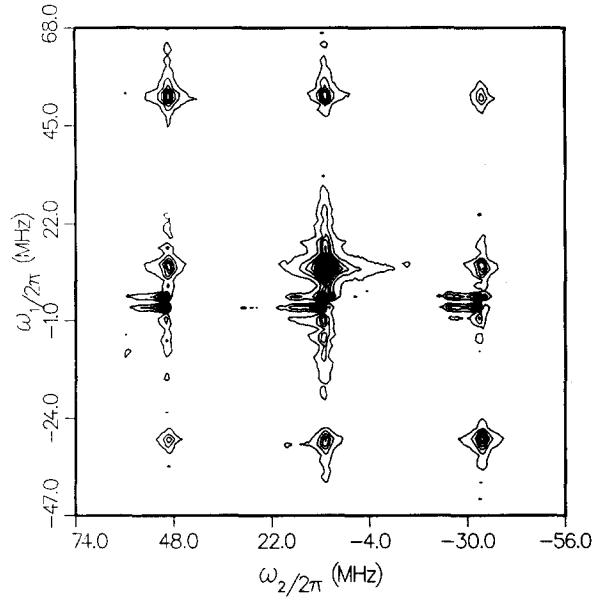

FIG. 9. 2D ELDOR contour map of spectrum of Fig. 7. Residual axial peaks appear as doublets centered on the line $\omega_1 = 0$; the observed splitting is an artifact of the base plane correction described in the text.

that of simple COSY except that three $\pi/2$ pulses are applied in the sequence: $\pi/2$–t_1–$\pi/2$–T–$\pi/2$–t_2 with the mixing time T being held constant. The application of this sequence (in NMR) to the study of chemically exchanging species was first illustrated by Jeener *et al.*[40] The basic pulse scheme for 2D ELDOR is illustrated in Fig. 7. The preparation and evolution periods are as described above for the COSY ESR experiment. During the mixing period, longitudinal magnetization components associated with each hf line can be exchanged, thereby mixing components carrying different precessional frequency information. The FID is recorded during the detection period as described for COSY ESR. A 2D ELDOR spectrum of 1.17×10^{-3} M PD-tempone in toluene-d_8 is shown in Fig. 8 with the corresponding contour map in Fig. 9. Magnetization transfer induced by Heisenberg spin exchange during the mixing period gives rise to cross correlations and hence to the appearance of cross peaks.[1] The cross peaks in Fig. 8 indeed have the characteristics predicted for an exchange process (cf. Sec. III). Measurement of the relative intensities of autopeaks and cross peaks gives a direct determination of the Heisenberg exchange rate ω_{HE} (cf. Sec. III).

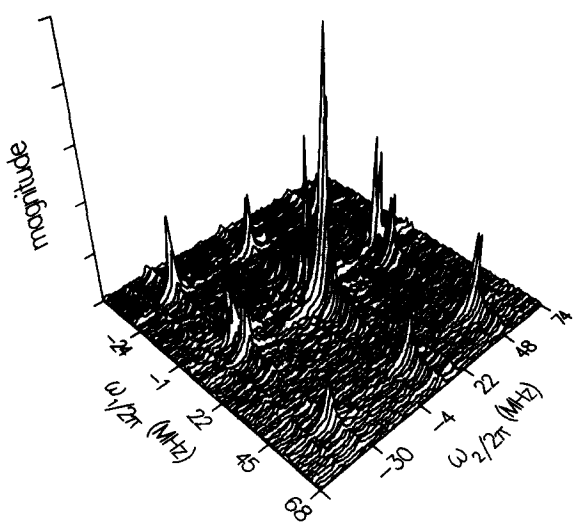

FIG. 8. Absolute value 2D ELDOR spectrum of 1.17×10^{-3} M PD-tempone in toluene-d_8 at 21°; $t_p = 15.2$ ns; $\Delta t_1 = 6$ ns; $\Delta t_2 = 3.9$ ns; $90t_1$ steps; 16 step phase alternation sequence with 30 averaged FID per step; dead time in t_2 of 100 ns; dead time in t_1 of 120 ns; mixing time $T = 3.10\times10^{-7}$ s; 256 complex data points per FID extending to 1 μs; acquisition time 27 min.

Quantitative determination of exchange rates with 2D ELDOR is complicated by the presence of unwanted coherences which add intensity only to the autopeaks; a phenomenon known as transverse interference.[41] Transverse interference arises from transverse magnetization following the first $\pi/2$ pulse which freely precesses for the rest of the sequence and interferes with the FID recorded during the detection period. A two step phase alternation sequence has previously been suggested for the cancellation of transverse interference.[41] We combine this sequence with our eight step 2D image cancellation sequence to obtain the 16 step procedure tabulated in Table II. The first four steps implement the CYCLOPS image cancellation sequence. Steps (5) through (8) generate the sequence 90,0,0 necessary for 2D quadrature detection. Cancellation of transverse interference and reduction of axial peaks[41] is accomplished with the sequence 180,180,0 implemented in steps (9) through (16). Another 2D ELDOR phase alternation sequence achieves these same cancellations in only eight steps (see Appendix B), and with a significant reduction in data collection time.

2D ELDOR spectra of 1.17×10^{-3} M PD-tempone in toluene-d_8 were recorded at 21 °C with the above 16 step phase alternation sequence for four different mixing times. Table III tabulates the ω_{HE} determined by comparison of autopeak and cross peak magnitudes in each of these spectra according to the theory of Sec. III. We prepared six different

TABLE II. Phase alternation sequence for 2D ELDOR.

Step	Phase[a]			Memory address[b]			
	ϕ_1	ϕ_2	ϕ_3	1	2	3	4
1	x	x	x	+1	+2		
2	y	y	y	−2	+1		
3	$-x$	$-x$	$-x$	−1	−2		
4	$-y$	$-y$	$-y$	+2	−1		
5	y	x	x			+1	+2
6	$-x$	y	y			−2	+1
7	$-y$	$-x$	$-x$			−1	−2
8	x	$-y$	$-y$			+2	−1
9	$-x$	$-x$	x	+1	+2		
10	$-y$	$-y$	y	−2	+1		
11	x	x	$-x$	−1	−2		
12	y	y	$-y$	+2	−1		
13	$-y$	$-x$	x			+1	+2
14	x	$-y$	y			−2	+1
15	y	x	$-x$			−1	−2
16	$-x$	y	$-y$			+2	−1

[a] The phase of each MW pulse in the three pulse sequence.
[b] There are four distinct arrays into which data from the two digitizer channels are either added (+) or subtracted (−).

concentrations of PD-tempone (PDT) in toluene-d_8 and determined T_2 ($M_I = 0$) for each by fitting the ESE envelope to a single exponential (see Appendix A); the results are tabulated in Table IV. The least squares fit to the T_2 vs [PDT] curve intercepted the [PDT] = 0 axis at $T_2(0) = 3.43 \pm 0.23 \times 10^{-7}$ s, representing the homogeneous Lorentzian linewidth in the absence of Heisenberg spin exchange.[42] An estimate of $\omega_{HE} = 4.25 \pm 0.60 \times 10^6\ s^{-1}$ for the $1.17 \pm 0.12 \times 10^{-3}$ M sample was obtained using the expression

$$2\omega_{HE}/3 = T_2^{-1}(HE) - T_2^{-1}(0), \tag{18}$$

where T_2(HE) is the T_2 in the presence of exchange and $T_2(0)$ is the T_2 in its absence.[42,43] Equation (18) is valid in the regime $\gamma_e \mathscr{A}_D \ll \omega_{HE} \ll \gamma_e \mathscr{A}_N$, where $\mathscr{A}_D$ and $\mathscr{A}_N$ correspond to the ^{2}H and ^{14}N hf splittings in G.[44,45] The exchange rate determined by ESE corresponds to the rate constant $k_{HE} = 3.63 \pm 0.63 \times 10^9\ M^{-1}\ s^{-1}$ (which agrees with the value of $\sim 3.1 \times 10^9\ M^{-1}\ s^{-1}$ reported in Ref. 46). The result is in agreement, within the experimental uncertainty, with the value determined by 2D ELDOR (on one of the same samples) of $\omega_{HE} = 4.65 \pm 0.19 \times 10^6\ s^{-1}$, corresponding to $k_{HE} = 3.97 \pm 0.43 \times 10^9\ M^{-1}\ s^{-1}$.

TABLE III. Dependence of T_2 on spin–probe concentration from ESE measurements.

[PD-tempone] (M)	T_2 (s)
2.57×10^{-4}	3.21×10^{-7}
5.10×10^{-4}	2.69×10^{-7}
8.78×10^{-4}	1.83×10^{-7}
1.02×10^{-3}	1.95×10^{-7}
1.17×10^{-3}	1.74×10^{-7}
1.44×10^{-3}	1.51×10^{-7}

TABLE IV. Measured ω_{HE} for different mixing times T from 2D ELDOR.

T (s)	ω_{HE} (s^{-1})[a]
2.70×10^{-7}	4.49×10^6
3.10×10^{-7}	4.89×10^6
3.30×10^{-7}	4.53×10^6
3.50×10^{-7}	4.71×10^6

[a] HE frequency obtained upon averaging the six values given by utilizing Eq. (50) for each cross peak of the 2D ELDOR spectrum.

The 2D ELDOR technique constitutes a direct observation of Heisenberg exchange, whereas the ESE technique is somewhat indirect; that is, one usually fits T_2^{-1} to a linear dependence on concentration, but this is not always valid.[42,44,47] Electron–electron dipolar (EED) relaxation between probe molecules can also contribute to the observed T_2 in a concentration dependent fashion. EED is ELDOR active,[48] but its presence is reflected relatively more substantially in the T_2^{-1}, hence also in the widths with respect to ω_1 and ω_2 of the 2D ELDOR resonance lines.[49] This allows for discrimination between HE and EED in the 2D ELDOR experiment (EED was *not* important in this experiment in a nonviscous solvent[42,50]). Finally we note that in an ELDOR experiment the sensitivity to ω_{HE} depends upon the ratio ω_{HE}/W_e (where W_e is the electron spin–flip rate), whereas in a T_2 experiment it depends upon $\omega_{HE} T_2(0)$, so that when $W_e \ll T_2(0)^{-1}$, as is frequently the case, the ELDOR experiment would be the more sensitive to ω_{HE}. In this connection, one should note that, whereas cw ELDOR only yields ratios such as ω_{HE}/W_e, time domain ELDOR, such as 2D ELDOR, yields the relaxation rates directly.[48,51,52]

Quantitative 2D ELDOR studies in general require the comparison of 2D absorption peak volumes, rather than peak amplitudes, as it is the former which correctly reflects the population difference at the end of the mixing period, whereas the latter is affected by differences in hf linewidths. In the present case, it is a good approximation to compare absolute value peak amplitudes, because the three hf lines of the observed spectrum have nearly equal width [we did find for the 1.17×10^{-3} M sample with $T = 3.10 \times 10^{-7}$ s a value of $4.58 \times 10^6\ s^{-1}$ for ω_{HE} determined from volume integrals of the pure 2D absorption line shapes; cf. Sec. III, Eq. (50)]. In the present experiment we have chosen a sample and temperature for which nuclear spin relaxation is negligible.[50] If the nuclear spin relaxation rate W_n constitutes a nonnegligible source of spin relaxation, then a more general analysis of the 2D ELDOR experiment is required (cf. Sec. III). A normal-mode analysis of the electron spin transitions[7,51,53] is applicable to the 2D ELDOR technique, and it may be used to obtain W_n, ω_{HE}, and the electron spin relaxation rate W_e. Thus one can truly think of 2D ELDOR as a two-dimensional form of electron–electron double resonance spectroscopy.

Refocussing coherence into an echo allows us to perform spin echo correlation spectroscopy[1] (SECSY). The objective of SECSY ESR is the determination of T_2 and any variation of T_2 across the spectrum. We have found from field-swept methods that the two-dimensional line shapes one obtains with 2D-ESE are highly sensitive to models of

molecular tumbling.[5] The advantage of SECSY in comparison to field-swept 2D-ESE is the order-of-magnitude shorter data acquisition time. In addition, SECSY has the potential for observing (weak) cross correlations which cannot be observed with techniques using narrowband excitation.

III. THEORY

A. General

A full density matrix formulation of the theory for 2D ELDOR follows from a theoretical study of ESE by Schwartz *et al.*[9,53,54] based upon the general time-domain analysis of spin relaxation by Freed.[51] The physics of the problem is described by the stochastic Liouville equation (SLE), which simultaneously includes the reversible quantum-mechanical spin dynamics and the irreversible molecular dynamics (usually treated classically). The time dependence of the transverse magnetization components is expressed by the density matrix elements that are off-diagonal in the electron spin state (call them Z_{ij}). The FID following a single pulse is given by the expression

$$s(t) = \sum_j a_j \exp(-\Lambda_j t), \tag{19}$$

where the complex coefficients a_j are given by

$$a_j = \sum_{lm} U_l O_{o,lj} O_{o,mj} U_m \tag{20}$$

and where $\mathbf{O}_o$ and $\mathbf{\Lambda}$ are the eigenvector and eigenvalue matrices associated with the SLE matrix governing the time evolution of the Z_{ij}, and $\mathbf{U}$ is the vector of (appropriately averaged) spin transition moments. The imaginary parts of the Λ_j represent the resonance frequencies $\omega_j = \mathrm{Im}(\Lambda_j)$, while the real parts represent the homogeneous widths $T_{2,j}^{-1} = \mathrm{Re}(\Lambda_j)$.

The time dependence of the longitudinal magnetization components is carried by the density matrix elements which are diagonal in the electron spin state.[55] We associate the matrix $\mathbf{O}_d$ with the transformation that diagonalizes the SLE matrix governing the evolution of the instantaneous population differences; the τ_m are the associated real eigenvalues. We refer to the space spanned by the $\mathbf{O}_d$ as the diagonal subspace, and that spanned by the $\mathbf{O}_o$ as the off-diagonal subspace. The pulses are assumed to effect an instantaneous rotation of the density matrix, thereby coupling the diagonal and off-diagonal subspaces. Having established concepts and necessary notation we write, without explicit derivation (but see Refs. 7, 9, 51, and 53), the expression for 2D ELDOR as

$$s'_{\mathrm{ELDOR}}(T,t_1,t_2) = B' \sum_{lmn} c'_{lmn} \times \exp(-\Lambda_n t_2)\exp(-T/\tau_m) \times \mathrm{Re}\left[\sum_j b_{lj} \exp(-\Lambda_j t_1)\right], \tag{21}$$

where

$$c'_{lmn} = \sum_{kr} U_r O_{o,rn} O_{o,kn} O_{d,km} O_{d,lm} \tag{22}$$

and

$$b_{lj} = \sum_p O_{o,lj} O_{o,pj} U_p. \tag{23}$$

The τ_m may be thought of as the decay times for the normal modes associated with the transfer of magnetization among the dynamic spin packets.[9]

Equations (21)–(23) represent only one of several terms predicted by the theory; in particular, they represent the contribution to the 2D spectrum which provides the ELDOR information. The remaining contributions are addressed in the rest of this discussion. We identify four independent contributions to the time-domain spectral function $s(T,t_1,t_2)$,

$$s_{(x,x,x)}(T,t_1,t_2) = s'_{\mathrm{ELDOR}} + s'_{\mathrm{Transverse}} + s'_{\mathrm{Axial}(E)} + s'_{\mathrm{Axial}(M)}, \tag{24}$$

where (x,x,x) identifies, for each pulse, the axis of rotation of the density matrix. s'_{ELDOR} is the contribution described in Eqs. (21)–(23), while $s'_{\mathrm{Transverse}}$ is the contribution associated with transverse interference, and $s'_{\mathrm{Axial}(E)}$ and $s'_{\mathrm{Axial}(M)}$ are the terms associated with axial peaks. The quadrature component is written analogously as

$$s_{(y,x,x)}(T,t_1,t_2) = s''_{\mathrm{ELDOR}} + s''_{\mathrm{Transverse}} + s''_{\mathrm{Axial}(E)} + s''_{\mathrm{Axial}(M)}. \tag{25}$$

In the case of Fig. 8, corresponding to the motionally narrowed regime with three well-separated hf lines, our expressions are greatly simplified by the fact that $\mathbf{O}_o = \mathbf{I}$, and we can write them as

$$s'_{\mathrm{ELDOR}}(T,t_1,t_2) = B' \sum_{nmj} c_{nmj} A_n(t_2) \times \exp(-T/\tau_m)\mathrm{Re}[A_j(t_1)] \tag{26}$$

and

$$s'_{\mathrm{ELDOR}}(T,t_1,t_2) = B' \sum_{nmj} c_{nmj} A_n(t_2) \times \exp(-T/\tau_m)\mathrm{Im}[A_j(t_1)], \tag{27}$$

where $A_i(t)$ is defined by

$$A_i(t) = \exp(-\Lambda_i t). \tag{28}$$

The real coefficients c_{nmj} are defined by

$$c_{nmj} = U_n O_{d,nm} O_{d,jm} U_j \tag{29}$$

with[56]

$$O_{d,nm} = \begin{array}{c} \\ -1 \\ 0 \\ 1 \end{array} \begin{array}{c} \begin{array}{ccc} 1 & 2 & 3 \end{array} \\ \begin{pmatrix} 3^{-1/2} & 2^{-1/2} & 6^{-1/2} \\ 3^{-1/2} & 0 & -2(6)^{-1/2} \\ 3^{-1/2} & -2^{-1/2} & 6^{-1/2} \end{pmatrix} \end{array} \tag{30}$$

and with $n = M_I = -1,0,1$ and $\tau_1^{-1} = 2W_e$, $\tau_2^{-1} = (2W_e + W_n + \omega_{\mathrm{HE}})$, and $\tau_3^{-1} = (2W_e + 3W_n + \omega_{\mathrm{HE}})$.[51,56] The U_n in Eq. (29) are given by $U_n = -i\epsilon/2$ where $-\epsilon$ is the equilibrium population difference for an isotropic system, given by $g\beta_e H_0 / k_B T$ in the high-field limit. We see immediately from Eqs. (26) and (27) that the effect of the 2D quadrature phase alternation scheme is to select the real part of

the time-domain spectral function $A_j(t_1)$ in the case of s' and the imaginary part in the case of s''. Similarly we obtain

$$s'_{\text{Transverse}}(T,t_1,t_2) = -B' \sum_n U_n^2 A_n(t_2) \times \text{Re}[A_n(T)]\,\text{Re}[A_n(t_1)] \quad (31)$$

and

$$s''_{\text{Transverse}}(T,t_1,t_2) = -B' \sum_n U_n^2 A_n(t_2) \times \text{Re}[A_n(T)]\,\text{Im}[A_n(t_1)]. \quad (32)$$

We can identify $s_{\text{Transverse}}$ as the transverse magnetization following pulse 1 which freely precesses for the rest of the pulse sequence, i.e., transverse interference. It is important to note the absence of cross terms in Eqs. (31) and (32), with the implication that only the amplitudes of the 2D ELDOR autopeaks are altered by transverse interference. To verify this result it is useful to examine the COSY ESR spectrum of Fig. 6. The expressions for COSY ESR are simply related to Eqs. (31) and (32) by eliminating all T dependence to obtain

$$s'_{\text{COSY}}(t_1,t_2) = -B' \sum_n U_n^2 A_n(t_2)\text{Re}[A_n(t_1)] \quad (33)$$

and

$$s''_{\text{COSY}}(t_1,t_2) = -B' \sum_n U_n^2 A_n(t_2)\text{Im}[A_n(t_1)]. \quad (34)$$

Equations (33) and (34) predict a COSY spectrum without cross peaks, consistent with the experimental result of Fig. 6. Given sufficiently rapid exchange, $\mathbf{O}_0$ is no longer simply the identity operator $\mathbf{I}$ and cross peaks are predicted to appear in the COSY spectrum.

The axial peaks arise from the two independent contributions $s_{\text{Axial}(E)}$ and $s_{\text{Axial}(M)}$ associated with electron spin flips during the evolution period and mixing period, respectively. Expressions for the axial peaks are

$$s'_{\text{Axial}(E)}(T,t_1,t_2) = s''_{\text{Axial}(E)} = B'[1-\exp(-2W_e t_1)] \times \sum_n U_n^2 A_n(t_2)\text{Re}[A_n(T)] \quad (35)$$

and

$$s'_{\text{Axial}(M)}(T,t_2) = s''_{\text{Axial}(M)} = B'[1-\exp(-2W_e T)] \times \sum_n U_n^2 A_n(t_2). \quad (36)$$

We see from Eqs. (35) and (36) that the precessional frequency information associated with $A_n(t_1)$ has been destroyed by the electron spin flips. The only remaining t_1 dependence of this magnetization is the recovery factor contained in $s_{\text{Axial}(E)}$; $s_{\text{Axial}(M)}$ is completely independent of t_1 and will appear as a base plane offset after FT with respect to t_2.

Upon FT with respect to t_2 we obtain $\hat{s}_{(x,x,x)}(T,t_1,\omega_2)$ and $\hat{s}_{(y,x,x)}(T,t_1,\omega_2)$ at which time we form[1]

$$\hat{s}(T,t_1,\omega_2) = \text{Re}[\hat{s}_{(x,x,x)}] + i\,\text{Re}[\hat{s}_{(y,x,x)}]. \quad (37)$$

FT with respect to t_1 yields the 2D spectrum given by

$$\text{Re}[S(T,\omega_1,\omega_2)] = S_{\text{ELDOR}} + S_{\text{Transverse}} + S_{\text{Axial}(E)} + S_{\text{Axial}(M)}, \quad (38)$$

where

$$S_{\text{ELDOR}}(T,\omega_1,\omega_2) = B' \sum_{nmj} c_{nmj}\,\text{Re}\left(\frac{1}{i\omega_2-\Lambda_n}\right) \times \text{Re}\left(\frac{1}{i\omega_1-\Lambda_j}\right) \times \exp(-T/\tau_m), \quad (39)$$

$$S_{\text{Transverse}}(T,\omega_1,\omega_2) = -B' \sum_n U_n^2\,\text{Re}\left(\frac{1}{i\omega_2-\Lambda_n}\right) \times \text{Re}\left(\frac{1}{i\omega_1-\Lambda_n}\right)\text{Re}[A_n(T)], \quad (40)$$

$$S_{\text{Axial}(E)}(T,\omega_1,\omega_2) = -\sqrt{2}\,\text{Re}\left(\frac{1}{i\omega_1-2W_e}\right) \times \sum_n U_n^2\,\text{Re}\left(\frac{1}{i\omega_2-\Lambda_n}\right) \times \text{Re}[A_n(T)], \quad (41)$$

$$S_{\text{Axial}(M)}(T,\omega_1,\omega_2) = B'[1-\exp(-2W_e T)]h(\omega_1) \times \sum_n U_n^2\,\text{Re}\left(\frac{1}{i\omega_2-\Lambda_n}\right), \quad (42)$$

where

$$h(\omega_1) = \mathcal{F}\{H(t_1^f - t_1)\}_{\omega_1}, \quad (43)$$

where $H(x)$ is the usual heaviside function, which vanishes for $x<0$ and is equal to 1 for $x>0$, and t_1^f is the final value of t_1. The entire τ_m dependence of $S(T,\omega_1,\omega_2)$ is carried by S_{ELDOR} as defined in Eq. (39). In order to estimate the τ_m from the experimental 2D spectrum we must separate S_{ELDOR} from the contributions described by Eqs. (40)–(42). Repeating the above calculation for different rotations about the axes in the rotating frame, we find that

$$s_{(-x,-x,x)}(T,t_1,t_2) = s'_{\text{ELDOR}} - s'_{\text{Transverse}} - s'_{\text{Axial}(E)} + s'_{\text{Axial}(M)} \quad (44)$$

and

$$s_{(-y,-x,x)}(T,t_1,t_2) = s''_{\text{ELDOR}} - s''_{\text{Transverse}} - s''_{\text{Axial}(E)} + s''_{\text{Axial}(M)}. \quad (45)$$

Upon coaddition of the FID following the sequence $(90°)_x$–t_1–$(90°)_x$–T–$(90°)_x$–t_2 with one following $(90°)_{-x}$–t_1–$(90°)_{-x}$–T–$(90°)_x$–t_2 we effect a cancellation of $S_{\text{Transverse}}$ and of $S_{\text{Axial}(E)}$. We have not found it possible, by phase cycling with only the quadrature phases 0°, 90°, 180°, and 270°, to effect a cancellation of all three contributions described in Eqs. (40)–(42). Addition of FIDs as described above is performed during data acquisition. We are left with the one remaining term $S_{\text{Axial}(M)}$ to remove during data analysis. To effect this removal, we first note that $s'_{\text{Axial}(M)}(T,t_2)$ given by Eq. (36) is independent of t_1, and it constitutes the only contribution to $s_{(x,x,x)}(T,t_1,t_2)$ with this

property. Thus we first estimate a constant baseplane offset in $\hat{s}_{(x,x,x)}(T,t_1,\omega_2)$, which we identify with $\hat{s}'_{\text{Axial}(M)}(T,\omega_2)$. Then we subtract this baseplane from $\hat{s}_{(x,x,x)}(T,t_1,\omega_2)$, and repeat this procedure with $\hat{s}_{(y,x,x)}$ prior to FT with respect to t_1. This procedure eliminates the large contribution of the form $h(\omega_1)\sim\sin\omega_1 t/\omega_1 t$ found in Eq. (42). The experimental implementation of the described phase alternation and base line correction schemes are not perfect, and thus there is residual amplitude in the experimental 2D ELDOR spectra associated with Eqs. (40)–(42). Most of this residual amplitude is associated with axial peak contributions, and it gives rise to the distortions seen along $\omega_1=0$ in the spectra of Figs. 6 and 8. Additional distortions near $\omega_1=0$ arise from the extra amplitude modulation in t_1 due to distortions in the second MW pulse (causing a variation of the rotation angle β for this pulse) as a function of interpulse delay t_1, which is a problem analogous to that in NMR.[17]

B. Off-resonance effects

We make an empirical correction to Eqs. (39)–(42) for off-resonance effects. We account for the reduction in amplitude of resonances for which $|\text{Im}(\Lambda_j)-\gamma_e B_0|>|\gamma_e B_1|$ by incorporating a factor V_j for each rotation which reflects the effective B_1 at the resonance frequency $\text{Im}(\Lambda_j)$. Combining Eqs. (29) and (39) we obtain

$$S_{\text{ELDOR}}(T,\omega_1,\omega_2)$$
$$=B'\sum_{nmj}U_n V_n\,\text{Re}\left(\frac{1}{i\omega_2-\Lambda_n}\right)U_j V_j^2$$
$$\times\text{Re}\left(\frac{1}{i\omega_1-\Lambda_j}\right)O_{d,nm}O_{d,jm}\exp(-T/\tau_m). \quad (46)$$

For the purpose of simulation we need only compute Eq. (46).

We have neglected inhomogeneous broadening in the above analysis, as it does not play a significant role in the interpretation of 2D ELDOR data given in this report (other than to broaden each resonance line by a small amount). The effect of including inhomogeneous broadening in the theory is that there would be five additional terms for Eqs. (24) and (25), reflecting three spin echoes associated with each pair of pulses, plus a stimulated echo and a twice refocused echo. (These matters are discussed elsewhere.[5,53]) These are the terms which would be important for slow motional 2D ELDOR spectra, where $T_2^*<\tau_d$, so an FID technique would not be appropriate. Instead, one could observe the stimulated echo, which has a structure very similar to that of Eqs. (21)–(23) (cf. Sec. IV).

C. Determination of W_e, W_n, and ω_{HE}

There are two procedures for the determination of relaxation rates from the 2D ELDOR data utilizing Eq. (46). One procedure is to collect several 2D ELDOR spectra at incremental values of the mixing time T, and directly observe the time evolution of each 2D spectral line. This data may be fit to the sum of exponentials, τ_m by nonlinear least squares to obtain W_e, W_n, and ω_{HE}. Let us illustrate typical behavior with T from our data in a simple fashion. Average cross-peak and autopeak amplitudes are tabulated in Table V for the four spectra associated with Table IV. Their behavior is qualitatively correct; autopeaks decay monotonically in T, whereas cross peaks first increase due to exchange and then decay as a result of electron spin flips. That this behavior is anticipated from the theory can be illustrated by inserting the appropriate τ_m into Eq. (46) (cf. Ref. 56) and simplifying to obtain for the special case of $W_n=0$:

$$A(T)\propto\exp(-2W_eT)+2\exp[-(2W_e+\omega_{\text{HE}})T] \quad (47)$$

for the autopeaks, and

$$C(T)\propto\exp(-2W_eT)-\exp[-(2W_e+\omega_{\text{HE}})T] \quad (48)$$

for the cross peaks. Obviously many data points in T are required if the data is to be fit to these expressions.

TABLE V. Average normalized cross-peak and autopeak amplitudes for series of mixing times T; $c_{mj}=a_{mj}V_j^3$.

T(s)	$\bar{c}_{jj}$	$\bar{c}_{mj,m\neq j}$
2.70×10^{-7}	0.395	0.227
3.10×10^{-7}	0.329	0.260
3.30×10^{-7}	0.312	0.235
3.50×10^{-7}	0.286	0.222

A second approach is based upon examining each 2D spectrum and comparing relative peak heights of the auto and cross peaks. This turns out to be a particularly convenient approach leading to simple analytical expressions for ω_{HE} and W_n when Eq. (30) is applicable. We illustrate this with the 2D ELDOR spectrum of Fig. 8 since it represents a particularly simple case for determination of ω_{HE}, given W_n is negligible, T_2 is nearly uniform across the spectrum, and the assumptions of Ref. 56 are appropriate (cf. Ref. 50). In this case we write the analytical expression, derived from Eq. (46), which relates ω_{HE} to the observed peak amplitudes. The normalized amplitude of a cross peak at position $\omega_1=\omega_j,\omega_2=\omega_m$ is related to the amplitude of the autopeak at $\omega_1=\omega_2=\omega_j$ with a proportionality factor a_{mj} by

$$\tfrac{1}{3}V_m V_j^2\exp(-2W_eT)[1-\exp(-\omega_{\text{HE}}T)]$$
$$=\tfrac{1}{3}a_{mj}V_j^3\exp(-2W_eT)[1+2\exp(-\omega_{\text{HE}}T)]. \quad (49)$$

The W_e factor conveniently drops out (so a knowledge of W_e is not needed nor obtained) after which some algebra leads us to the expression

$$\omega_{\text{HE}}=\frac{1}{T}\ln\left(\frac{2a_{mj}V_j+V_m}{V_m-a_{mj}V_j}\right). \quad (50)$$

The V_i are determined by the amplitudes of the autopeaks (which go as V_i^3) and the a_{mj} are the appropriate ratios of observed cross-peak to autopeak amplitudes as already defined. Equation (50) (and its generalization for $W_n\neq0$) applies also to the case where T_2 varies across the spectrum if we compare volume integrals of 2D ELDOR absorption lines rather than amplitudes. Equation (50) was utilized in Sec. II to obtain ω_{HE} from our 2D ELDOR data.

IV. DISCUSSION AND CONCLUSIONS

We have illustrated how our Fourier transform ESR spectrometer is capable of routine use in a number of applications. It is our objective to develop the technique to be applicable to all studies involving nitroxides. At the present time we are limited to the application of FT methods to spectra not exceeding about 100 MHz spectral bandwidth. We have illustrated applications of the FT technique that do not require uniformity of B_1 across the entire spectrum. B_1 uniformity is not a necessity for the implementation of most two-dimensional techniques. B_1 nonuniformity can be accounted for in simulations by recognizing that spectral components which are only partially rotated by the pulses have reduced effective transition moments,[7] as we have done. We have illustrated the utility of two-dimensional correlation spectroscopy as a double resonance technique which yields quantitative information without necessarily requiring simulation or least-squares fitting of the data.[57] It was shown that a simple two pulse COSY experiment is insensitive to Heisenberg exchange provided $\omega_{HE} \ll \mathscr{A}_N$, whereas a three pulse sequence, sensitive to the instantaneous population differences, is highly sensitive to exchange-driven magnetization transfer.

In the application of this technique to slow-tumbling motions of nitroxides we would obtain all of the ELDOR data in a single 2D spectrum. Such spectra would yield information about the couplings between spin packets corresponding to different molecular orientations which can provide insight on the microscopic details of the motional process.[5,8,9,51] The implementation of a 2D ELDOR experiment for the study of slow-tumbling motions would be somewhat different than described for motionally narrowed systems. FIDs in these systems are, in general, rapidly damped as a result of inhomogeneous static fields which are not averaged by the motion as in the motionally narrowed spectra. The FID will, in general, be lost in the dead time following a MW pulse. In these instances the transverse magnetization can still be refocused into a spin echo. In the 2D ELDOR experiment one would have the option of applying an additional refocusing pulse or of recording the stimulated echo following the third pulse. The latter method would have the advantage that axial peaks will not be refocused and therefore cannot contribute intensity to the 2D ELDOR spectrum. In another application, the implementation of SECSY to slow-tumbling nitroxides would be identical to the method previously described[1] for motionally narrowed spectra, except that reduction of the dc magnetic field homogeneity is not required. This SECSY application would be the 2D FT analog of the field-swept 2D experiment described in Ref. 5. It would have the advantages of (i) greatly reduced data acquisition times; (ii) pulse widths significantly shorter than the relevant T_2 's. Many other possibilities exist for the application of other two-dimensional spectroscopies to ESR.

Access to the full range of the nitroxide spectra with FT techniques will require at least a doubling of our present spectrometer bandwidth. The main challenge is the generation of sufficiently large B_1 fields at the sample. Based upon our current experience a 220 MHz spectrum would require at least a 14 G B_1 field at the sample in a rectangular pulse of width about 6 ns. We have the ability to generate pulses of this width, but not sufficient power to rotate on-resonant magnetization by $\pi/2$ in a low Q cavity resonator. The implementation of a loop-gap resonator, which has been stabilized against electric breakdown,[23] should enable the generation of a 25 G B_1 at the sample because of the high conversion efficiency of these resonators.[22,58] In order to make the field more uniform across the spectrum, the possibility of using shaped pulses[59] is being investigated. A nearly rectangular pulse shape is used only as a matter of convenience; the response of the magnetization to such a pulse is of the form $\sin(\omega t_p)/\omega t_p$ and is far from optimal for FT work because of the points of null response.[4] Shaping of pulses can contain all of the available MW power within a single band or envelope, thus improving the conversion of MW power into useful B_1. Other possibilities for improvement of the present spectrometer include the fabrication of a high sweep rate 200 MHz digitizer using available high-speed device technology. We predict a reduction in FID acquisition time by at least an order-of-magnitude with the implementation of such digitizers. Also under investigation is the design of a multifrequency FT spectrometer taking advantage of new multioctave stripline devices.

In cases where B_1 field strengths are insufficient for total spectral coverage, variations of the techniques described in this report may be of interest. These are techniques of two-dimensional correlation spectroscopy which require that only a limited region of the spectrum be irradiated (so-called "soft-COSY" techniques[60]). A soft 2D ELDOR spectra would provide information about the couplings among only those spin packets rotated by the MW pulse. In these experiments one could collect several such 2D spectra, each focusing on a different region of the spectrum, and then combine the data during data analysis. Related techniques are already frequently utilized in NMR for 2D nuclear Overhauser spectroscopy of systems of biological interest.

It is clear that full bandwidth irradiation techniques will be limited to specific suitable applications in ESR which will probably not, for the foreseeable future, include transition metals in liquid solution. Transition metal spectra have bandwidths of up to several gigahertz requiring B_1 's of several hundred Gauss, and their T_2 's in liquids are too short (typically less than or on the order of nanoseconds). The methods described in this report are generally applicable to studies of organic free-radicals, however, because their spectral bandwidths usually do not exceed 100–200 MHz, and their T_2 's are usually significantly greater than a nanosecond. Finally, we believe that the range of applications of 2D FTESR to chemical physics will continue to increase as new developments in high-speed electronics, resonators, and microwave devices find their way into the research lab.[61]

APPENDIX A

All samples of PD-tempone in toluene-d_8 were derived from a 2×10^{-3} M stock solution by successive dilution; estimated uncertainty in probe concentration: $\pm$ 10%. Samples were degassed by the freeze/thaw method and sealed in 8 mm NMR sample tubes purchased from Norrel Inc.. Toluene-d_8 (99% D) was purchased from Aldrich Chem. Co.

TABLE VI. Eight step phase alternation sequence for 2D ELDOR.

Step	Phase[a]			Memory address[b]			
	ϕ_1	ϕ_2	ϕ_3	1	2	3	4
1	x	x	x	+1	+2		
2	y	y	y	−2	+1		
3	x	x	$-x$	−1	−2		
4	y	y	$-y$	+2	−1		
5	y	x	x			+1	+2
6	$-x$	y	y			−2	+1
7	y	x	$-x$			−1	−2
8	$-x$	y	$-y$			+2	−1

[a] The phase of each MS pulse in the three pulse sequence.
[b] There are four distinct arrays into which data from the two digitizer channels are either added (+) or subtracted (−).

and PD-tempone was synthesized by Igner. The sample volume contained within the TE102 cavity was 1 cm^3, filling $\sim 1/8$ of the cavity. For determination of T_2 by ESE the FID was quenched by reduction of the dc field homogeneity; each echo envelope consisted of 256 equally spaced points with 8 or 10 ns resolution and a τ_d of 64 ns; pulsewidths were 36 and 57 ns. 2D data matrices were padded with zeroes to twice the record length in t_2 (512 complex points) and to 128 points in t_1 prior to Fourier transformation using a modified Cooley–Tukey FFT algorithm. All spectra were collected at ambient temperature in a temperature controlled laboratory maintained at 21 ± 0.5 °C.

APPENDIX B

We have recently discovered a more compact phase alternation sequence for 2D ELDOR which achieves the same result as the 16 step sequence but requires only 8 steps. The eight step sequence is tabulated in Table VI. Comparison of Tables II and VI reveals that the 8 step sequence is just a subset of the 16 step sequence. This does not imply, however, that the remaining 8 steps of the 16 step sequence are redundant, but only that they are not essential for the observation of 2D ELDOR. In the 16 step sequence for 2D ELDOR and in the 8 step sequence for 2D COSY, the basic repeating unit is the 4 step CYCLOPS sequence necessary even for 1D spectroscopy. In the eight step 2D ELDOR sequence this unit has been abandoned in lieu of a more compact four step sequence which accommodates the 180,180,0 sequence for cancellation of transverse interference. To understand this contraction, we must recognize that the 180,180,0 sequence inverts the phase of the magnetization associated with type E axial peaks and transverse interference, leaving all other components unchanged, whereas the 180,180,180 sequence used in the standard CYCLOPS inverts the phase of all magnetization. The 180,180,180 sequence is a requirement of CYCLOPS in order to eliminate dc offsets in the FIDs. The sequence 0,0,180 has the opposite effect from the 180,180,0 sequence, in that transverse interference and axial type E magnetization is unchanged, while all other magnetization is inverted in phase. Thus if we replace the 180,180,180 sequence in CYCLOPS by 0,0,180, then the cancellation of dc offsets in the FIDs is accompanied by removal of signal associated with type E axial peaks and transverse interference. We have found that spectra obtained with the 8 step sequence are superimposable (within experimental uncertainty) on the same spectra collected with the full 16 step sequence. The advantage of halving the number of steps in this sequence is the reduction in data collection time from 27 min in the case of Fig. 8 to about 17 min for an analogous experiment using the eight step sequence. The large impact on data collection time reflects the large amount of overhead associated with transferring commands and data between the LSI11 and the spectrometer instrumentation.

[1] J. Gorcester and J. H. Freed, J. Chem. Phys. **85**, 5375 (1986).
[2] J. Gorcester, G. L. Millhauser, and J. H. Freed, Proc. XXIII Congress Ampere on Magnetic Resonance, Rome (1986), p. 562.
[3] M. Bowman, Bull. Am. Phys. Soc. **31**, 524 (1986).
[4] J. P. Hornak and J. H. Freed, J. Magn. Reson. **67**, 501 (1986).
[5] G. L. Millhauser and J. H. Freed, J. Chem. Phys. **81**, 37 (1984).
[6] L. Kar, G. L. Millhauser, and J. H. Freed, J. Phys. Chem. **88**, 3951 (1984).
[7] G. L. Millhauser, J. Gorcester, and J. H. Freed, in *Electronic Magnetic Resonance of the Solid State*, edited by J. A. Weil (Canada Chemical Society, Ottowa, 1987), p. 571.
[8] G. L. Millhauser, Ph.D. thesis, Cornell University, 1986.
[9] L. J. Schwartz, G. L. Millhauser, and J. H. Freed, Chem. Phys. Lett. **127**, 60 (1986).
[10] If the Q of the resonator is above $\sim$200 there is no advantage to using the PIN diode switches since the resonator will admit a pulse of no less than $\sim$15 ns duration [see Ref. 13, Eq. (7a)] and the modified TWT amplifier can generate pulses of this width.
[11] C. Dunnam, J. Gorcester, and J. H. Freed (in preparation)
[12] C. P. Poole, *Electron Spin Resonance, A Comprehensive Treatise on Experimental Techniques* (Interscience, New York, 1967).
[13] W. B. Mims, Rev. Sci. Instrum. **36**, 1472 (1965).
[14] B. C. Henderson and J. A. Cook, Microwave Systems News **17**, 75 (1987).
[15] D. I. Hoult and R. E. Richards, Proc. R. Soc. London Ser. A **344**, 311 (1975).
[16] R. M. Bracewell, *The Fourier Transform and Its Applications*, 2nd ed. (McGraw–Hill, New York, 1986).
[17] A. F. Mehlkopf, D. Korbee, T. A. Tiggelman, and R. Freeman, J. Magn. Reson. **58**, 315 (1984).
[18] (a) S. E. Bialkowski, Rev. Sci. Instrum. **58**, 695 (1987); (b) S. L. Nickolaisen and S. E. Bialkowski, J. Chem. Info. Comp. Sci. **26**, 57 (1986).
[19] With many interleaving oscilloscopes (e.g., LeCroy 9400) the effective sampling rate cannot be varied, i.e., the scope either samples at the rate of the internal analog-to-digital converters, or it interleaves to obtain the maximum available effective sampling rate; the mode of operation is determined by the chosen sweep time (i.e., time/division).
[20] For sampling rates of no higher than 100 Ms/s, the DSP technology model 2101 signal averager achieves very high sweep rates (2000 sweeps/s for 1024 points/sweep). A 200 Msample/s *effective* sampling rate could be achieved with the DSP 2101 by advancing the trigger by 5 ns after each sweep, but with an accompanying reduction in effective sweep rate.
[21] W. B. Mims, in *Electron Paramagnetic Resonance*, edited by S. Geschwind (Plenum, New York, 1972).
[22] (a) W. Froncisz and J. S. Hyde, J. Magn. Reson. **47**, 515 (1982); (b) J. P. Hornak and J. H. Freed, *ibid.* **62**, 311 (1985).
[23] B. R. Johnson, Ph.D. thesis, Cornell University, 1984; B. R. Johnson, J. S. Denker, N. Bigelow, L. P. Levy, J. H. Freed, and D. M. Lee, Phys. Rev. Lett. **52**, 1508 (1984).
[24] R. R. Ernst, G. Bodenhausen, and A. Wokaun, *Principles of Nuclear Magnetic Resonance in One and Two Dimensions* (Oxford University, New York, 1987).
[25] See Ref. 24, Eqs. (4.2.26).
[26] R. Ernst and W. A. Anderson, Rev. Sci. Instrum. **37**, 93 (1966).
[27] R. Ernst, Adv. Magn. Reson. **2**, 1 (1966).
[28] Hewlett Packard HP54111 digitizing oscilloscope, obtained on loan courtesy of Hewlett Packard.
[29] J. S. Waugh, J. Mol. Spectrosc. **35**, 298 (1970).

[30]Matched filtering doubles the Lorentzian linewidth.

[31]This estimate is based on a 1 kW 10 ns transmitter pulse and a noise temperature of 5000 K.

[32]For the echo we have $(S/NT)^{1/2} \propto Q^{1/2} \exp(-2\tau_d/T_2)$ consistent with $Q_{\rm opt} = \omega T_2/128$, or $Q_{\rm opt} = 50$ and $\tau_d \simeq 25$ ns for a $T_2 = 100$ ns and $\nu = 10$ GHz.

[33]The signal voltage at the detector associated with an FID Fourier component of frequency ω [call it $V_s(\omega)$] is reduced by a factor of $1/\sqrt{2}$ for ω equal to a resonator half-power point frequency $\omega_{\rm rf} \pm \omega_{\rm rf}/2Q$, i.e., $V_s(\omega_{\rm rf} \pm \omega_{\rm rf}/2Q) = V_s(\omega_{\rm rf})/\sqrt{2}$.

[34]R. G. Kooser, W. V. Volland, and J. H. Freed, J. Chem. Phys. **50**, 5243 (1969).

[35]More generally one should include a geometric factor in Eq. (17), associated with the microwave field distribution in the resonator [see Ref. 34, Eqs. (2.2) and (2.3)]. For our immediate purpose, it is sufficient to use the simplified expression of Eq. (17).

[36]W. P. Aue, E. Bartholdi, and R. R. Ernst, J. Chem. Phys. **64**, 2229 (1976).

[37]J. Keeler and D. Neuhaus, J. Magn. Reson. **63**, 454 (1985).

[38]D. J. States, R. A. Haberkorn, and D. J. Ruben, J. Magn. Reson. **48**, 286 (1982).

[39](a) Such mechanisms can induce "off-diagonal" relaxation-matrix elements between the different transitions (Refs. 45 and 48). (b) Actually, by linear predictive methods (Ref. 57, and references therein) *very weak* cross peaks are obtained.

[40]J. Jeener, B. H. Meier, P. Bachmann, and R. R. Ernst, J. Chem. Phys. **71**, 11 (1979).

[41]S. Macura and R. R. Ernst, Mol. Phys. **41**, 95 (1980).

[42](a) M. P. Eastman, R.G. Kooser, M. R. Das, and J. H. Freed, J. Chem. Phys. **51**, 2690 (1969); (b) M. P. Eastman, G. V. Bruno, and J. H. Freed, *ibid.* **52**, 2511 (1970).

[43]A. E. Stillman and R. N. Schwartz, Mol. Phys. **32**, 1045 (1976).

[44]A. E. Stillman and R. N. Schwartz, J. Magn. Reson. **22**, 269 (1976).

[45]J. H. Freed, J. Phys. Chem. **71**, 38 (1967).

[46]R. N. Schwartz, L. L. Jones, and M. K. Bowman, J. Phys. Chem. **83**, 3429 (1979).

[47]A. Nayeem, Ph.D. thesis, Cornell University, 1986.

[48]J. H. Freed in *Multiple Electron Resonance Spectroscopy*, edited by M. Dorio and J. H. Freed (Plenum, New York, 1979), Chap. 3.

[49]Thus, for the case of a three line nitroxide in the motional narrowing regime one has (Refs. 42 and 48) [see also: D. S. Leniart, H. D. Connor, and J. H. Freed, J. Chem. Phys. **63**, 165 (1975); A. Abragam, *The Principles of Nuclear Magnetism* (Oxford University, London, 1961)] that HE contributes the amount $\omega_{\rm HE}$ to the overall exchange rate $\omega_{\rm EX}$, [i.e., we let $\omega_{\rm EX} = \omega_{\rm HE} + \omega_{\rm EED}$, (cf. Ref. 56)], whereas EED contributes the amount $\omega_{\rm EED} = AJ(0)$ [with $A = (19/36)(1/3)\hbar^2\gamma_e^4$ and $J(0) = 32\pi^2 n\eta/25kT$ with n the number density of nitroxides and η the viscosity for a simple diffusion model]. The term $\omega_{\rm EED}$ is from the $S_{1\pm}S_{2\mp}$ terms for radicals contributing to different hf lines. The contributions to the linewidth are however $(T_2^{-1})_{\rm HE} = 2\omega_{\rm HE}/3$ and $(T_2^{-1})_{\rm EED} = 19\omega_{\rm EED}/3$, because of the large secular $(S_{1z}S_{2z})$ contribution for EED.

[50]J. S. Hwang, R. P. Mason, L. P. Hwang, and J. H. Freed, J. Phys. Chem. **79**, 489 (1975).

[51]J. H. Freed, J. Phys. Chem. **78**, 1155 (1974); in *Time Domain Electron Spin Resonance*, edited by L. Kevan and R. N. Schwartz (Wiley Interscience, New York, 1979).

[52]J. Yin, M. Pasenkiewicz-Gierula, and J. S. Hyde, Proc. Natl. Acad. Sci. **84**, 964 (1987).

[53]L. J. Schwartz, Ph.D. thesis, Cornell University, 1984; L. J. Schwartz and J. H. Freed (to be published).

[54]L. J. Schwartz, A. E. Stillman, and J. H. Freed, J. Chem. Phys. **77**, 5410 (1982).

[55]This is the case for well-separated hf lines. More generally the pseudo-diagonal elements are also required (Refs. 48 and 53).

[56]These are the results appropriate when the nonsecular contributions from the g-tensor, hf tensor, and EED tensor may be neglected. More generally, up to five τ_m would be required in Eqs. (21)–(23) for a nitroxide (Refs. 48 and 51). The presence of chemical exchange and/or pseudosecular EED terms would lead to an effective exchange frequency $\omega_{\rm EX}$ replacing $\omega_{\rm HE}$ in these expressions (Ref. 48).

[57]We did find, however, that least-squares fitting in the form of linear prediction [J. Gorcester and J. H. Freed, J. Magn. Reson. (in press)] is a convenient method for projection of the pure 2D absorption representation of 2D ELDOR data, necessary for determination, of volume integrals of the 2D absorption lines. It can also be effectively utilized to remove artifacts, such as residual axial peaks, and to significantly improve the signal to noise.

[58]W. Froncisz (private communication).

[59]W. S. Warren, J. Chem. Phys. **81**, 5437 (1984).

[60]R. Brüschweiler, J. C. Madsen, C. Griesinger, O. W. Sørensen, and R. R. Ernst, J. Magn. Reson. **73**, 380 (1987).

[61]*Note added in proof*: The generalization of Eq. (50) for $W_n \neq 0$ has been successfully utilized to accurately obtain the W_n in another system where it is important.